Int. J. Electrochem. Sci., 11 **(2016)** 3179 - 3189

International Journal of
ELECTROCHEMICAL
SCIENCE
www.electrochemsci.org

One-pot Synthesis of radial ZnO microparticles deposited on graphene nanosheets as the Anode Materials for Lithium-Ion Batteries

Yan Zhao[1,2], *Haipeng Li*[1,2,3], *Yongguang Zhang*[1,2,*], *Hongxian Xie*[1,2], *Fuxing Yin*[1,2,**]

[1] Research Institute for Energy Equipment Materials, Hebei University of Technology, Tianjin 300130, China
[2] Tianjin key laboratory of materials laminating fabrication and interface control technology, Hebei University of Technology, Tianjin 300130, China
[3] School of Material Science & Engineering, Hebei University of Technology, Tianjin 300130, China
[*]E-mail: yongguangzhang@hebut.edu.cn
[**]E-mail: foxing2008@hotmail.co.jp

Received: 20 September 2015 / *Accepted:* 19 January 2016 / *Published:* 1 March 2016

A novel ZnO/graphene nanosheet (ZnO/GN) composite has been successfully synthesized by a facile one-pot hydrothermal method. ZnO micro-particles, with the quasi-spherical radial morphology, are uniformly deposited on the wrinkled GN. According to the hydrothermal method used and characterization results observed, the formation process is proposed. When adopted as anodes for lithium-ion batteries, the ZnO/GN composite shows enhanced cyclability and rate capability compared with the pristine ZnO counterpart. The ZnO/GN electrode could yield a discharge capacity of 620 mAh g^{-1} at the 2nd cycle with the corresponding coulombic efficiency of 71 % over 100 cycles at 0.2 A g^{-1}. In addition, the ZnO/GN composite exhibits a good rate capability with discharge capacity of 132 mAh g^{-1} at high current density of 3.2 A g^{-1}. This improved electrochemical performance stems from the positive combinative effects of both radial microparticle structure of ZnO and GN additives, wherein radial ZnO microparticle provides a large surface with a short ion transport and electrolyte diffusion length and GN renders a flexible robust conductive matrix, buffering the large volume changes during the charge/discharge processes.

Keywords: lithium ion battery; ZnO/graphene nanosheet composite; anode; one-pot hydrothermal; energy storage

1. INTRODUCTION

As a most popular used anode material for lithium ion batteries (LIBs), graphite possesses a theoretical capacity of 372 mAh g^{-1} [1]. However, facing the ever increasing demands of EV industry,

the current graphite anode cannot satisfy the energy and power requirement, and many studies have explored the next generation of anode materials with larger specific capacities and higher energy densities [2, 3]. By replacing traditional graphite anode, metal oxides have been extensively investigated, due to their high theoretical capacities and safety [4]. Among various metal oxide candidates, ZnO has a unique alloying reaction combining with conversion reaction, as below, resulting in a high theoretical capacity of 978 mAh g^{-1} [5]:

$ZnO+2Li \rightleftarrows Zn+Li_2O$

$Zn+Li \rightleftarrows LiZn$

Total reaction: $ZnO+3Li \rightleftarrows LiZn+Li_2O$

Furthermore, ZnO has other advantages, such as environmental benignity, chemically stable, facile preparation and low cost. However, in spite of these advantages, several drawbacks of ZnO anode have to be pointed out, mainly including: poor electrical conductivity and large volume and structure change during the charge/discharge process [6].

Recently, great efforts have been devoted to improve the electrochemical performance of ZnO anodes. Various nanostructures of ZnO, such as nanosheet, nanorod and nanospheres, have been synthesized, effectively alleviating the volume variation and shortening lithium ion diffusion length [7-9]. Furthermore, it has been well proven that metal oxide/carbon composite can present positive combinative effects between the metal oxide and the carbon material [10]. Thus, various carboneous materials, such as carbon nanotubes, mesoporous carbon and graphene, have been used to composite with ZnO as a buffering agent to restrain the mechanical degradation of ZnO particles and as a conducting medium to facilitate the electron transport and lithium-ion diffusion [11-14].

Among them, graphene, a two-dimensional, one-atom-thick nanosheet structural carbon materials with extraordinary electronic, thermal and mechanical properties has attracted a great deal of research attention [14]. Very recently, Yuan and coworkers synthesized radial ZnO microparticles assembled by numerous nanoparticles, which shows an improved electrochemical performance [15]. Inspired by this work, best to our knowledge, we firstly report on a facile one-pot method to prepare radial ZnO microparticles deposited on graphene nanosheets via hydrothermal process as the anode materials for lithium-ion batteries and its physical and electrochemical properties are also investigated.

2. EXPERIMENTAL PART

2.1. Material preparation

Graphene oxide (GO) was synthesized from natural flake graphite by a modified Hummers' method [16]. To prepare the expected ZnO/GN composite, 150 mg GO was firstly dispersed in a mixture of 10 mL deionized (DI) water and 10 mL ethanol with ultrasonic radiation to form a homogeneous brown solution. Subsequently, 15 mL of ethanol containing 150 mg of was $ZnNO_3 \cdot 6H_2O$ added to the above brown solution. After enduring ultrasonic radiation for 0.5 h, 300 mg of $CO(NH_2)_2$ dissolved in 15 mL of DI water was dropped to the mixture under vigorous stirring. After sonication again, the obtained homogeneous suspension was transferred into a 60 mL Teflon-lined stainless steel autoclave. The autoclave was sealed and maintained at 150 °C for 12 h and then cooled down to ambient temperature naturally. The resulting product was separated from the solution by

centrifugation, washed repetitively with distilled water and ethanol, and then dried at 80 °C under vacuum overnight. For comparison, a control experiment was performed to prepare bare ZnO using the same route without adding graphite oxide.

2.2. Material Characterization

Powder X-ray diffraction (XRD, Bruker D8 ADVANCE), using Cu Kα radiation was employed to identify the crystalline phases of the synthesized materials. Thermogravimetry (TG, SDT Q600, American TA Company) was applied under N_2 atmosphere to determine the components of the composite in the temperature range of 20-500 °C (10 °C min^{-1}). The morphologies and structure of the samples were investigated by scanning electron microscopy (SEM, FEI Quanta 400) and transmission electron microscopy (TEM, FEI Tecnai G^2 F20 S-TWIN) as well as selected area electron diffraction (SEAD) pattern, respectively.

2.3. Electrochemical measurements

The electrochemical performance of the samples was evaluated using 2025 coin cells assembled in a glove box filled with Ar. Working electrode were fabricated by painting slurry of 75 wt% as-prepared samples, 15 wt% acetylene black and 10 wt% polyvinylidene fluoride in 1-methyl-2-pyrrolidinone onto a circular piece of nickel foam with 12 mm in diameter. After drying under vacuum over night at 80 °C, the resulting film was pressed at 20 MPa to assure a good contact between active materials and Ni current collector. The active material loading in each electrode was about 1 mg cm^{-2}. A lithium disc was used as the counter electrode and reference electrode. The electrolyte was 1 M $LiPF_6$ dissolved in a mixture of dimethyl carbonate (DMC), diethyl carbonate (DEC) and ethylene carbonate (EC) at the ratio of 1:1:1 by volume, and the separator was microporous polypropylene film. The galvanostatic charge-discharge tests were carried out in a cut-off potential window of 0.005-3.0 V vs. Li/Li^+ at different current densities (LAND battery tester). Cyclic voltammetry (CV) was carried out in the potential range of 0-3.0 V vs. Li/Li^+ at a scan rate of 0.1 mV s^{-1} (CHI 660D electrochemical workstation). Electrochemical impedance spectroscopy (EIS) measurements was performed over the frequency range from 0.01 to 100 kHz with applied voltage amplitude of 10 mV (CHI 660D electrochemical workstation).

3. RESULTS AND DISCUSSION

Figure 1 shows the XRD patterns of ZnO, GN and ZnO/GN composite. The pure ZnO material possesses six obvious diffraction peaks at $2\theta = 31.8^o$, 34.4^o, 36.3^o, 47.5^o, 56.6^o, and 62.9^o, which are attributed to the reflections of (100), (002), (101), (102), (110), and (103) facets of the wurtzite hexagonal structured ZnO (space group P63mc, JCPDS No. 36-1451), respectively [17]. The GN displays a strong diffraction peak at around 26^o and a weak one at around 44^o, which can be ascribed to the (002) and (100) reflection of carbon, respectively (JCPDS 26-1077) [17]. In diffraction pattern of ZnO/GN composite, all characteristic peaks of ZnO and GN appears with lower intensity, which

indicates that ZnO is anchored on the surface or gaps of graphene layers in ZnO/GN composite. The XRD results indicate that the hydrothermal co-assembling method is effective in preparing ZnO/GN composite.

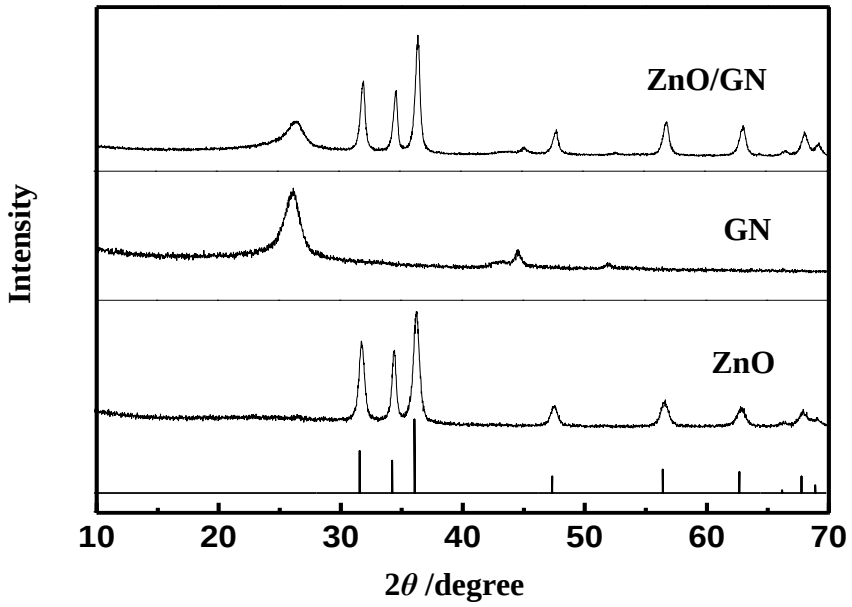

Figure 1. XRD patterns of the synthesized ZnO, GN, and ZnO/GN samples.

Figure 2a and c show typical gradually enlarged SEM images of ZnO, from which one can see that the obtained ZnO quasi-spherical particles have a uniform radial morphology. The diameter of each radial microsphere is about 3.0 μm. The morphology of ZnO/GN composite is shown in Figure 2b and d. ZnO particles still remain the basic quasi-spherical morphology, which are deposited on GNs to assemble the ZnO/GN composite.

As shown in Figure 3a, the ZnO microsphere has a several-branched radial structure. The size of the ZnO microsphere is about 3.0 μm, which agrees with the SEM results. The SAED pattern of ZnO (insert in Figure 3a) is composed of continuous polycrystalline rings and can be indexed with the hexagonal ZnO phase. Enlarged observation on the corner of the ZnO microsphere indicates that each branch is composed of numerous nanoparticles (Figure 3b). The rough surface of the ZnO particle is favorable for adhesion with GN sheets. Figure 3c shows the wrinkled and layered structured of GN, which is also favorable for adhesion with the rough ZnO particles. This trend is confirmed by TEM observation (Figure 3d). As can be seen in Figure 3d, the ZnO particles are deposited uniformly among wrinkled graphene nanosheets. The GNs could offer electron rapid transfer channels due to the electrons can transfer along the graphene nanosheets [14]. Furthermore, GN could render a flexible robust conductive matrix, buffering the large volume changes during the charge/discharge processes.

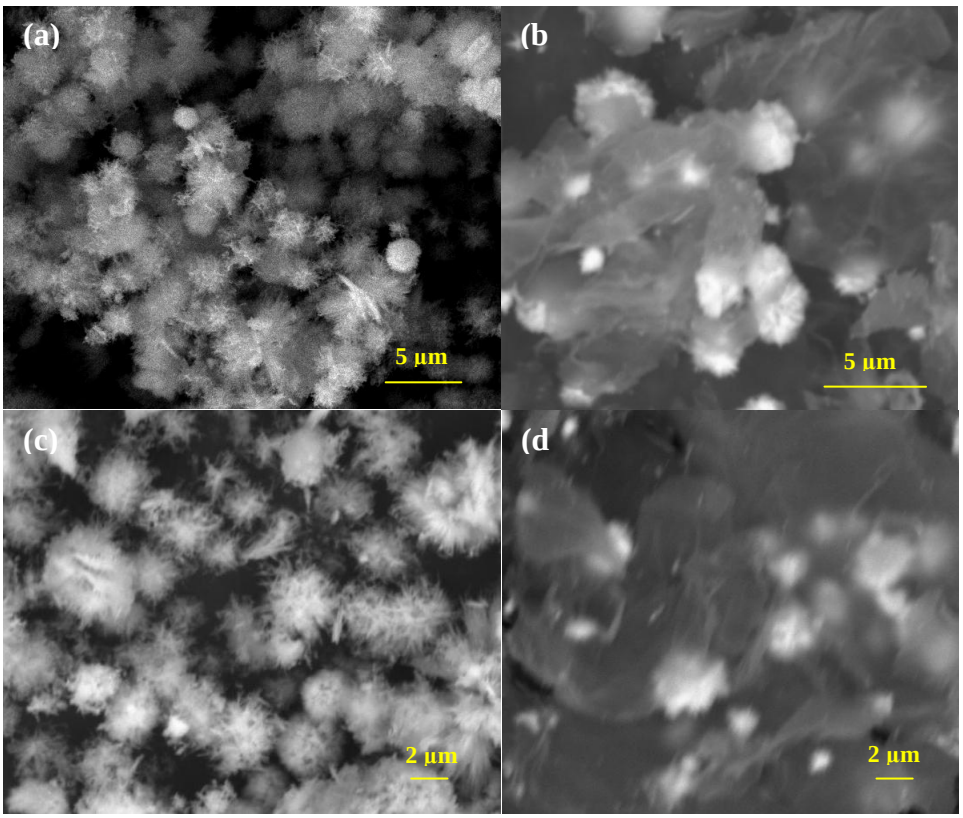

Figure 2. SEM images of (**a, c**) ZnO, and (**b, d**) ZnO/GN samples.

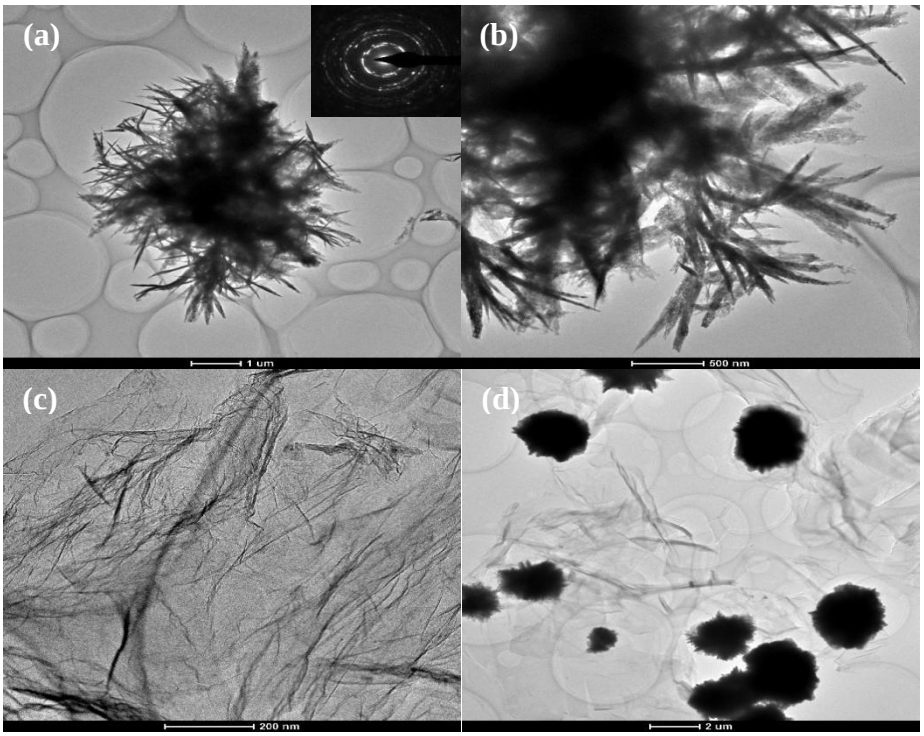

Figure 3. TEM images of (**a, b**) ZnO, (c) graphene, and (**d**) ZnO/GN composite.

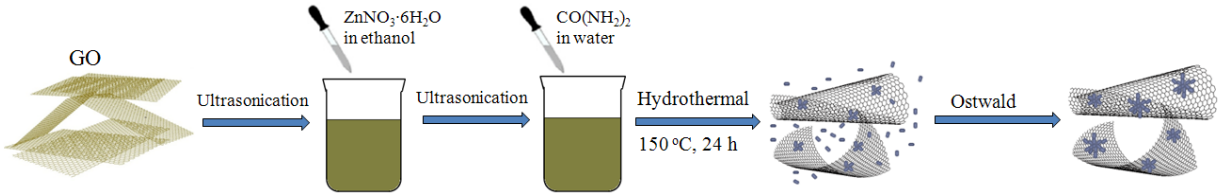

Scheme 1. Schematic for the formation process of the ZnO/GN composite.

Scheme 1 depicts the possible formation process of the ZnO/GN composite according to the hydrothermal method used and the micrography results obtained. On the one side, GO is reduced to GN and the GN sheets are twisted during the hydrothermal process. On the other side, in the hydrothermal environment, homogeneous nucleation of ZnO arose on the surface or in the gaps of the GN sheets and then crystallized momentarily to form nanoparticles with high-surface energy at the initial stage. Under super-critical conditions in autoclave, the original ZnO nanoparticles on the surface or in the gaps of the GN sheets became the crystallization centre. In the subsequent stage, the Ostwald ripening process occurs in the presence of water.

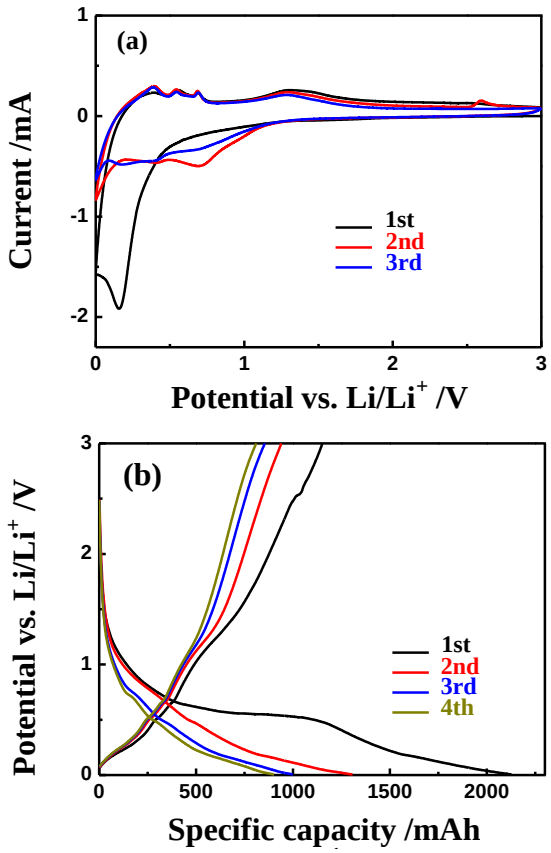

Figure 4. (**a**) CV curves of the ZnO/GN composite electrode, (**b**) Charge-discharge profiles of the ZnO/GN composite electrode at the current density of 100 mA g^{-1}.

Water might release lots of gas bubbles during the Ostwald ripening process, which made ZnO crystals slowly grew or aggregated along the crystallization centre on the surface or in the gaps of the

GN sheets to minimize the interfacial energy. The growth habit of the ZnO polar crystal makes it grow along with the direction of [0001]. The original crystallization centre is composed of several ZnO nanoparticles towards different directions, which final promote the ZnO crystals to form several-branched microparticles. As mentioned above, the rough surface of the ZnO particles and the wrinkled and layered structured of GN are favorable for adhesion. Thus, the ZnO/GN composite would be obtained due to their structural rigidity and the radial morphology of ZnO could be maintained.

The electrochemical properties of ZnO and ZnO/GN composite were tested by a 2025 coin cell. The CV profiles of ZnO/GN composite in the initial three cycles are shown in Figure 4a. The only one strong peak at ~0.2 V in the first cathodic scan can be ascribed to the formations of Li-Zn alloy and the solid electrolyte interphase (SEI) layer. The several different oxidation peaks at 0.3, 0.5, and 0.7 and 1.4 V in the subsequent anodic scan indicate the occurrence of a multi-step dealloying process of Li-Zn alloy, the decomposition of the organic-like-layer, and the decomposition of Li_2O [18]. The one peak at ~0.7 V in the second and third cathodic scans can be ascribed to the formations of Li-Zn alloy. After the first cycle, the CV curves exhibit good reproducibility and almost coincide in shape, showing high reversibility of the ZnO/GN composite.

Galvanostatic discharge-charge curves of the ZnO/GN electrode with a current density of 0.1 A $g^{-1}$are depicted in Figure 4b. The plateaus on the voltage profiles are in agreement with the CV data in Figure 4a. The ZnO/GN electrode delivers an initial discharge capacity of 2126 mAh g^{-1}, including the irreversible extra lithium storage during the SEI layer formation. The initial charge capacity is 1151 mAh g^{-1}. The ZnO/GN electrode delivers the discharge capacity of 1307 mAh g^{-1} during the second cycle. After the initial cycle, the discharge and charge curves tend to overlap, suggesting a relatively steady state of the lithiation/delithiation process. At the fourth cycle, the charge and discharge capacity of the electrode are 812 and 901 mAh g^{-1}, respectively. After four cycles, the coulombic efficiency has reached a point of 90%.

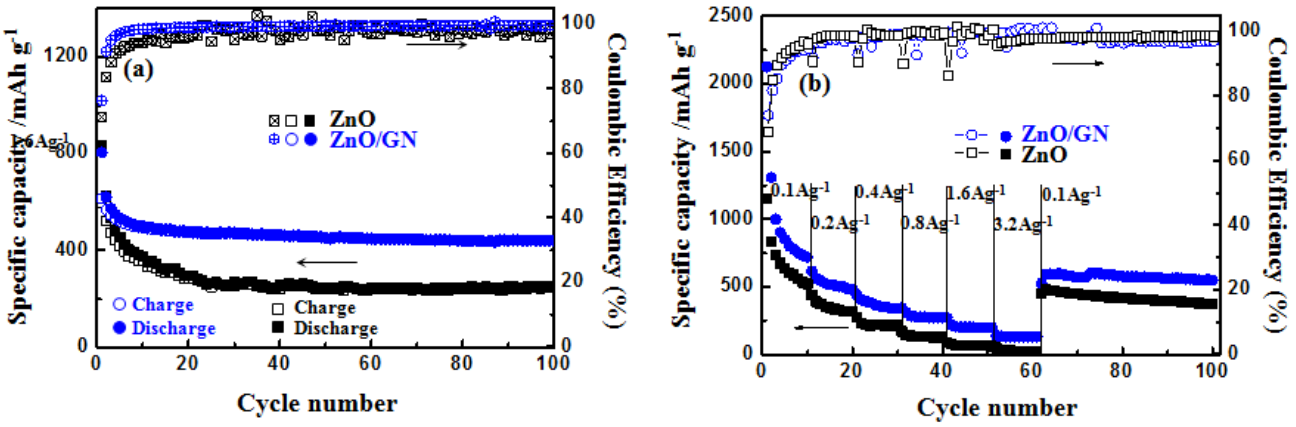

Figure 5. (**a**) Cycle performance and (**b**) rate capability of the ZnO and ZnO/GN electrodes.

Cyclability of ZnO and ZnO/GN composite is shown in Figure 5a. For ZnO/GN composite, the discharge and charge capacities decreased gradually at the initial 10 cycles at 0.2 A g^{-1}. After the 11th cycle, the ZnO/GN composite exhibits an enhanced cycling performance with a high coulombic

efficiency (above 99%). At 100 cycles, a large reversible capacity of 442 mAh g^{-1} is preserved, corresponding to about 88 % of the capacity retention from the 11th cycle, which indicates very stable reversibility of the electrochemical reactions and excellent capacity retention. For the ZnO electrode, capacity dropped dramatically and less than 260 mAh g^{-1} reversible capacity was gained after 100 cycle. This result clearly demonstrate that GN can effectively enhance the cycle performance of ZnO anode.

The kinetic behavior of the ZnO/GN composite is evaluated by rate capability test. The ZnO/GN composite show a better rate capability than ZnO counterpart. With the current densities increase from 0.1, 0.2, 0.4, 0.8, 1.6 to 3.2 A g^{-1}, the reversible capacities were 1307, 515, 367, 278, 203, 132, respectively.

Moreover, the capacity almost fully recovered when the discharge rate is switched back to 0.1 A g^{-1}, indicating an excellent rate capability of ZnO/GN composite. Compared with ZnO, ZnO/GN composite has better rate capability. This performance improvement could be attributed to that GN could provide convenient transport pathways for Li^+ and electrons and tolerate the volume expansion during the charge/discharge process, thereby, exhibiting good rate capability [19-21].

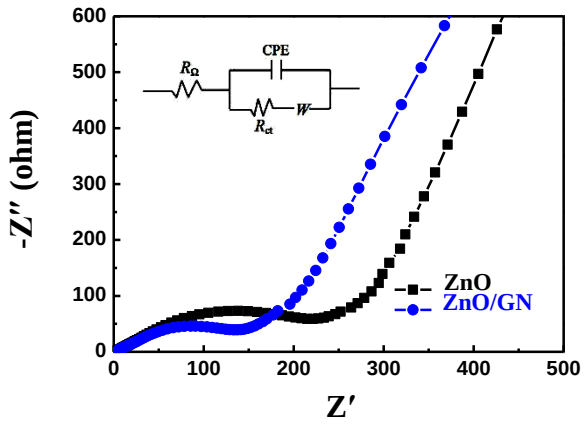

Figure 6. Nyquist plots of the ZnO and ZnO/GN electrodes after the first cycles with the whole frequency region of 100 kHz to 0.01 Hz.

Electrochemical impedance spectroscopy (EIS) measurement were conducted to study the conductivity and charge transfer behavior associate with the ZnO-based materials. As shown in Fig. 6, the comparative EIS data for the ZnO and ZnO/GN electrodes are conducted after the initial cycle. For both electrodes, the semicircle from the high frequency to medium frequency region represents the SEI film resistance and the charge transfer resistance on the interface between the electrode and the electrolyte [22,23]. Besides, the straight sloped line in the low frequency region corresponds to the lithium diffusion resistance inside the electrode [24]. A smaller high-to-medium frequency semicircle can been in the ZnO/GN composite EIS spectra compared with the ZnO counterpart, indicating a significant decrease in charge transfer resistance in ZnO/GN composite compared with ZnO. That is

due to that the introduction of GN not only impart good conductivity and high surface area for ZnO micropartcle to deposit, but also provide a robust electron transport framework [25].

Comparing with the electrochemical performances of other published ZnO/graphene anodes [26-30], as-prepared ZnO/graphene nanocomposite in our work shows desirable electrochemical performance, as shown in Table1. One can see that the values of reversible capacity and capacity retention at 100th cycles in our study are superior to other ZnO/graphene nanocomposite anodes, indicating the radial ZnO microparticles deposited on graphene nanosheets are promising high-performance anode for Li-ion batteries.

Table 1. Comparison of ZnO/graphene nanocomposite's anodes for Li-ion batteries performance with this work

Materials	nth cycle Reversible capacity (mAh g^{-1})	Capacity retention for n cycles (%)	Current density (mA g^{-1})	Potential (V vs. Li^+ /Li)	Reference
ZnO/ reduced graphene oxide	402 (100th)	23.3	200	0.0-3.0	[26]
ZnO/ graphene composites	404 (100th)	26.6	500	0.0-2.5	[27]
graphene/ ZnO composites	401 (30th)	34.7	100	0.0-3.5	[28]
ZnO-graphene composites	246 (100th)	14.9	100	0.0-3.0	[29]
ZnO/ graphene nanocomposite	300 (25th)	24.3	50	0.0-2.5	[30]
ZnO/graphene nanosheet	442 (100th)	88	200	0.0-3.0	Our work

4. CONCLUSION

In summary, we developed ZnO/GN composite as an anode in LIBs prepared by a facile one-pot hydrothermal method. In the ZnO/GN composite, the ZnO microspheres with several-branched

radial structure are homogeneously anchoring on graphene sheets. The ZnO/GN composite exhibits large reversible capacity, good cyclability and high rate capability, due to the improvement of electrical conductivity by well-defined contact between ZnO as an active material and GN as an excellent electronic conductor. Furthermore, GN works as a flexible conductive matrix, enhancing mechanical stabilities to tolerate the large volume changes during the charge/discharge processes.

ACKNOWLEDGEMENTS
The authors are grateful of financial support by the National Natural Science Foundation of China (Grant No. 21406052), Program for the Outstanding Young Talents of Hebei Province (Grant No. BJ2014010), Natural Science Foundation of Hebei Province of China (Project No. E2015202037) and Science and Technology Correspondent Project of Tianjin (Project No. 14JCTPJC00496). H. Xie is grateful of financial support by the Youth Foundation of Hebei Educational Committee (Grant No.QN2014094).

References

1. L.J. Fu, H. Liu, C. Li, Y.P. Wu, E. Rahm, R. Holze and H.Q. Wu, *Solid State Sci.*, 8 (2006) 113.
2. A. Birrozzi, R. Raccichini, F. Nobili, M. Marinaro, R. Tossici and R. Marassi, *Electrochim. Acta*, 137 (2014) 228.
3. A. Manthiram, *J. Phys. Chem. Lett.*, 2 (2011) 176.
4. J. Wu, C. Chen, Y. Hao and C. Wang, *Colloids Surf. A*, 468 (2015) 17.
5. G.H. Yuan, G. Wang, H. Wang and J.T. Bai, *Ionics*, 21 (2015) 365.
6. Y.N. Zhou, W.J. Li and Z.W. Fu, *Electrochim. Acta*, 59 (2012) 435.
7. X.H. Huang, X.H. Xia, Y.F. Yuan and F. Zhou, *Electrochim. Acta*, 56 (2011) 4960.
8. L. Xiao, D. Mei, M. Cao, D. Qu and B. Deng, *J. Alloys Compd.*, 627 (2015) 455.
9. F. Li, L. Yang, G. Xu, X.Q. Huang, X. Yang, X. Wei, Z. Ren, G. Shen and G. Han, *J. Alloys Compd.*, 577 (2013) 663.
10. F. Hao, Z. Zhang and L. Yin, *ACS Appl. Mater. Interfaces*, 5 (2013) 8337.
11. X.H. Huang, X.H. Xia, Y.F. Yuan and F. Zhou, *Electrochim. Acta*, 56 (2011) 4960.
12. H. Köse, Ş. Karaal, A.O. Aydın and H. Akbulut, *J. Power Sources*, 295 (2015) 235.
13. P. Li, Y. Liu, J. Liu, Z. Li, G. Wu and M. Wu, *Chem. Eng. J.*, 271 (2015) 173.
14. C.T. Hsieh, C.Y. Lin, Y.F. Chen and J.S. Lin, *Electrochim. Acta*, 111 (2013) 359.
15. G.H. Yuan, G. Wang, H. Wang and J.T. Bai, *Ionics*, 21 (2015) 365.
16. J.P. Zhao, S.F. Pei, W.C. Ren, L.B. Gao and H.M. Cheng, *ACS Nano*, 4 (2010) 5245.
17. G.H. Yuan, G. Wang, H. Wang and J.T. Bai, *J. Nanopart. Res.*, 17 (2015) 1.
18. C. Chen, H. Zhang, Y. Xu, M. Ji, H. Dong and C. Zhao, *RSC Adv.*, 5 (2015) 40219.
19. Y. Zhao, Z. Bakenova, Y. Zhang, H.F. Peng, H.X. Xie and Z. Bakenov, *Ionics*, 21 (2015) 1925.
20. Y. Zhang, Y. Zhao, A. Konarov, D. Gosselink, H.G. Soboleski and P. Chen, *J. Power Sources*, 241 (2013) 517.
21. Y. Zhang, Y. Zhao, Z. Bakenov, M.R. Babaa, A. Konarov, C. Ding and P. Chen, *J. Electrochem. Soc.*, 160 (2013) A1194.
22. Y. Zhang, Z. Bakenov, Y. Zhao, A. Konarov, T.N.L. Doan, M. Malik, T. Paron and P. Chen, *J. Power Sources*, 208 (2012) 1.
23. Y. Zhang, Y. Zhao, Z. Bakenov, M. Tuiyebayeva, A. Konarov and P. Chen, *Electrochim. Acta*, 143 (2014) 49.
24. Y. Zhou, X. Jiang, L. Chen, J. Yue, H. Xu, J. Yang, Y. Qian, *Electrochim. Acta*, 127 (2014) 252.
25. J. Li, K. Li, M. Li, D. Gosselink, Y. Zhang and P. Chen, *J. Power Sources*, 252 (2014) 107.

26. J. Wu, C. Chen, Y. Hao and C. Wang, *Colloid. Surface. A*, 468 (2015) 17.
27. L.L. Xu, S.W. Bian and K.L. Song, *J. Mater. Sci.*, 49 (2014) 6217.
28. Y. Zhao, G. Chen and Y. Wang, *J. Nanomater.*, 2014 (2014) 1.
29. M. Yu, A. Wang, Y. Wang, C. Li and G. Shi, *Nanoscale*, 6 (2014) 11419.
30. W.T. Song, J. Xie, S.Y. Liu, Y.X. Zheng, G.S. Cao, T.J. Zhu and X.B. Zhao, *Int. J. Electrochem. Sci.*, 7 (2012) 2164.